Inorg. Chem. **2008**, *47*, 1361−1369

Single-Crystalline $ZnGa_2O_4$ Spinel Phosphor via a Single-Source Inorganic Precursor Route

Lu Zou, Xu Xiang, Min Wei, Feng Li,* and David G. Evans

State Key Laboratory of Chemical Resource Engineering, P.O. Box 98, Beijing University of Chemical Technology, Beijing 100029, P.R. China

Received June 26, 2007

The synthesis of single-crystalline $ZnGa_2O_4$ spinel phosphor with intense ultraviolet-emitting properties through a novel single-source inorganic precursor route is reported. This synthetic approach involves the calcination of a Zn−Ga layered double hydroxide precursor followed by selective leaching of the self-generated zinc oxide. Material characterization has been presented by chemical analysis, X-ray diffraction analysis, thermogravimetric−differential thermal analysis, Fourier transform infrared spectroscopy, scanning electron microscopy, transmission electron microscopy, X-ray photoelectron spectroscopy, electron paramagnetic resonance, nuclear magnetic resonance, extended X-ray absorption fine structure analysis, UV–vis, and photoluminescence measurements. The results indicate that a single-crystalline $ZnGa_2O_4$ spinel with an average particle size of around 150 nm has been obtained at a lower calcination temperature and shorter calcination time compared with that with the high-temperature solid-state reaction method, based on the fact that the large amount of highly dispersed ZnO particles generated during the high-temperature calcination of the single-source inorganic precursor has a remarkable segregation and inhibition effect on the growth of $ZnGa_2O_4$ spinel. Furthermore, it has been confirmed that that Ga^{3+} ions locate not only on the octahedral sites but also on the tetrahedral sites in the matrix of the $ZnGa_2O_4$ spinel structure, and the Ga−O coordination environment has a great influence on the photoluminence of $ZnGa_2O_4$ phosphors.

Introduction

Zinc gallate ($ZnGa_2O_4$) phosphor has stimulated enormous attention in recent years due to its prospective applications in diverse areas including field emission display,[1] thin film electroluminescence display,[2] and vacuum florescent display.[3] As an oxide-based phosphor, it shows better chemical stability over existing sulfide phosphors and can endure a high electron beam current.[4] With a band gap energy (E_g) of 4.4 eV, $ZnGa_2O_4$ is a potentially transparent conducting oxide in the near-UV region[5] and exhibits a strong blue emission due to the transition via a self-activation center of Ga−O groups under excitation by both ultraviolet light and low-voltage electrons.[5,6] Moreover, their photoluminescence properties can be tuned via doping transition metal or rare earth ions.[7]

At present, various synthetic approaches of $ZnGa_2O_4$ spinel using either metal oxides or metal-containing complexes as precursors have been employed. The most commonly used route is the solid-state reaction between ZnO and Ga_2O_3.[1,3,5b,6,8] This approach usually requires several cycles of heat-treating at considerably elevated temperatures for a long time, which leads to side-reactions such as ZnO volatilization and thus gives nonstoichiometric

* Author to whom correspondence should be addressed. Tel.: 8610-64451226. Fax: 8610-64425385. E-mail: lifeng_70@163.com.

(1) Tran, T. K.; Park, W.; Tomm, J. W.; Wagner, B. K.; Jacobsen, S. M.; Summers, C. J.; Yocom, P. N.; McClelland, S. K. *J. Appl. Phys.* **1995**, *78*, 5691.

(2) Minami, T.; Kuroi, Y.; Takata, S. *J. Vac. Sci. Technol. A* **1996**, *14*, 1736. (b) Flynn, M.; Kitai, A. H. *J. Electrochem. Soc.* **2001**, *148*, 149. (c) Minami, T.; Kuroi, Y.; Miyata, T.; Yamada, H.; Tanaka, S. *J. Lumin.* **1997**, *72*, 997.

(3) (a) Itoh, S.; Toki, H.; Sato, Y.; Morimoto, K.; Kishino, T. *J. Electrochem. Soc.* **1991**, *138*, 1509. (b) Shea, L. E.; Datta, R. K.; Brown, J. J., Jr. *J. Electrochem. Soc.* **1994**, *141*, 2198.

(4) Vecht, A.; Smith, D. W.; Chadha, S. S.; Gibbons, C. S. *J. Vac. Sci. Technol., B* **1994**, *12*, 781.

(5) (a) Hsieh, I. J.; Chu, K. T.; Yu, C. F.; Feng, M.S. J. *Appl. Phys.* **1994**, *76*, 3735. (b) Omata, T.; Ueda, N.; Ueda, K.; Kawazoe, H. *Appl. Phys. Lett.* **1994**, *64*, 1077.

(6) (a) Shea, L. E.; Datta, R. K.; Brown, J. J., Jr. *J. Electrochem. Soc.* **1994**, *141*, 1950. (b) Jeong, I.-K.; Park, H. L.; Mho, S.-I. *Solid State Commun.* **1998**, *105*, 179.

(7) (a) Yu, C. F.; Lin, P. *J. Appl. Phys.* **1996**, *79*, 7191. (b) Kim, J. S.; Kim, J. S.; Kim, T. W.; Park, H. L.; Kim, Y. G.; Chang, S. K.; Han, S. D. *Solid State Commun.* **2004**, *131*, 493. (c) Yu, M.; Lin, J.; Zhou, Y. H.; Wang, S. B. *Mater. Lett.* **2002**, *56*, 1007. (d) Xu, Z.; Li, Y.; Liu, Z.; Wang, D. *J. Alloys Compd.* **2005**, *391*, 202.

10.1021/ic7012528 CCC: $40.75
Published on Web 01/15/2008

products. Liquid-phase synthesis (coprecipitation,[9] hydrothermal,[10] sol–gel,[7c,11] etc.) is an alternative method and generally leads to the formation of $ZnGa_2O_4$ phosphors with homogeneous particles at a relatively lower synthesis temperature than that of the solid-state method. However, there are only a few reported studies on the preparation of fine $ZnGa_2O_4$ powders by the liquid-phase synthesis route,[9,10a,b,11a] and in some cases, the surface contamination of phosphors due to the introduction of organic reagents should not be ignored. Therefore, it has always been a challenge to develop a new synthesis route for $ZnGa_2O_4$ spinels with consideration of affordability and versatility.

Layered double hydroxides (LDHs) are synthetic layered anionic clays,[12] in which the divalent and trivalent metal cations are octahedrally coordinated with hydroxyl groups to form two-dimensional brucite-like layers that are stacked together through electrostatic interactions with interlayer anions. Within the brucite-like layers, the cations are uniformly distributed *on an atomic level* without the segregation of "lakes" of separate cations.[13] The calcination of LDHs is known to give spinels, but these are always mixed with the divalent metal oxide.[12a] This reflects the fact that, in LDHs, the ratio M^{II}/M^{III} is usually[12a] in the range 2–4, whereas in a spinel, the required ratio is $M^{II}/M^{III} = 0.5$. Recently, we reported the formation of zinc aluminate ($ZnAl_2O_4$) spinels with mesopore networks through two stages of calcination and successive leaching of chemical components starting from a ZnAl−LDH precursor.[14] The two-phase $ZnO/ZnAl_2O_4$ composite first form upon the calcination of ZnAl−LDH at 500 °C or above, and then mesopores form through alkali leaching of self-generated ZnO from the composite.

In this contribution, we study the uniform synthesis of a single-crystalline $ZnGa_2O_4$ phosphor using a ZnGa−LDH precursor, based on the idea that the large amount of highly dispersed ZnO formed during the calcination of ZnGa−LDH, as a sacrificial template, has a remarkable segregation and inhibition effect on the growth of single-crystalline $ZnGa_2O_4$ spinel. We also characterize the structure of resultant $ZnGa_2O_4$ phosphor using a combination of nuclear magnetic resonance (NMR), electron paramagnetic resonance (EPR), and extended X-ray absorption fine structure (EXAFS) measurements, which endow us with a further understanding of the relationship between $ZnGa_2O_4$ structures and their photoluminescence properties.

Experimental Section

Synthesis of ZnGa−LDH Precursor. The single-source layered precursor (ZnGa−LDH) was synthesized by a coprecipitation method. $Zn(NO_3)_2{\cdot}6H_2O$ (analytical reagent, A.R.; 60 mmol) and $GaCl_3$ (99.99%; 20 mmol) were dissolved in 100 mL of deionized water to give solution A. NaOH (A.R.) and Na_2CO_3 (A.R.) were dissolved in 100 mL of deionized water to give a mixed base solution, B. The concentrations of the base were related to those of the metal ions in solution A as follows: $[CO_3^{2-}] = 2.0\ [Ga^{3+}]$, $[OH^-] = 1.6\ ([Zn^{2+}] + [Ga^{3+}])$. Solution A and solution B were simultaneously added dropwise to a four-necked flask containing 50 mL of deionized water at room temperature. The pH value was held constant at 10.0 ± 0.1. The resulting suspension was further aged at 85 °C for 20 h with stirring, recovered by four dispersions and centrifugation cycles with deionized water, and finally dried at 70 °C overnight. Elem. anal. found % (Calc. for $[Zn_{0.77}Ga_{0.23}(OH)_2](CO_3)_{0.115}{\cdot}0.82H_2O$): Zn, 41.05 (41.24); Ga, 13.35 (13.14); H_2O, 12.09 (12.10); Zn/Ga, 3.28 (3.34).

Synthesis of $ZnGa_2O_4$ Spinel. The above-synthesized ZnGa−LDH precursor was calcined in the air at 900 °C for 6 h with a heating rate of 10 °C/min. The resulting product was slowly cooled to room temperature and treated with a 10 M aqueous sodium hydroxide solution at 60 °C for 2 days under moderate stirring. The final products were separated by centrifugation and dried at 80 °C overnight.

For comparison, $ZnGa_2O_4$ spinel phosphor was also prepared by the solid-state reaction method. The starting materials were high-purity ZnO (99.99%) and Ga_2O_3 (99.999%). Stoichiometric amounts of the starting materials were thoroughly mixed, then heated in the air at 1100 °C for 16 h.

Characterization. Powder X-ray diffraction (XRD) patterns of the samples were recorded using a Shimadzu XRD-6000 diffractometer under the following conditions: 40 kV, 30 mA, graphite-filtered Cu Kα radiation ($\lambda = 0.15418$ nm). The samples, as unoriented powders, were step-scanned in steps of 0.04° (2θ) using a count time of 10 s/step. The observed diffraction peaks were corrected using elemental Si as an internal standard [d (111) = 0.31355 nm; JCPDS file no. 27-1402].

Elemental analysis was performed using a Shimadzu ICPS-7500 inductively coupled plasma emission spectrometer (ICP-ES). All samples were dried at 100 °C for 24 h prior to analysis, and solutions were prepared by dissolving the ZnGa−LDH sample in dilute hydrochloric acid (1:1) at room temperature and $ZnGa_2O_4$ samples in a dilute hydrochloric acid and nitric acid (1:3) mixed solution under hydrothermal conditions (120 °C for 24 h).

Thermogravimetric and differential thermal analyses (TG-DTA) were carried out in the air on a Perkin-Elmer Diamond thermal analysis system with a heating rate of 10 °C/min.

Room-temperature Fourier transform infrared (FT-IR) spectra were recorded in the range 400−4000 cm^{-1} with 2 cm^{-1} resolution on a Bruker Vector-22 Fourier transform spectrometer using the KBr pellet technique (1 mg of sample in 100 mg of KBr).

Hitachi S-3500N and S-4700 scanning electron microscopes (SEMs) and an EDAX Genesis 60 energy dispersive X-ray spectrometer (EDX) were employed to observe the morphology and analyze chemical composition. The accelerating voltage was 20 kV.

(8) (a) Ikarashi, K.; Sato, J.; Kobayashi, H.; Saito, N.; Nishiyama, H.; Inoue, Y. *J. Phys. Chem. B* **2002**, *106*, 9048. (b) Phani, A. R.; Santucci, S.; Di Nardo, S.; Lozzi, L.; Passacantando, M.; Picozzi, P.; Cantalni, P. *J. Mater. Sci.* **1998**, *33*, 3969. (c) Ohtake, T.; Sonoyama, N.; Sakata, T. *Chem. Phys. Lett.* **1998**, *298*, 395.

(9) Jung, H.-K.; Park, D.-S.; Park, Y. C. *Mater. Res. Bull.* **1999**, *34*, 43.

(10) (a) Hirano, M. *J. Mater. Chem.* **2000**, *10*, 469. (b) Hirano, M.; Imai, M.; Inagaki, M. *J. Am. Ceram. Soc.* **2000**, *83*, 977. (c) Li, Y.; Duan, X.; Liao, H.; Qian, Y. *Chem. Mater.* **1998**, *10*, 17. (d) Chen, L.; Liu, Y.; Lu, Z.; Huang, K. *Mater. Chem. Phys.* **2006**, *97*, 247.

(11) (a) Wu, S.-H.; Cheng, H.-C. *J. Electrochem. Soc.* **2004**, *151*, 159. (b) Sei, T.; Nomura, Y.; Tsuchiya, T. *J. Non-Cryst. Solids* **1997**, *218*, 135. (c) Daniele, S.; Tcheboukov, D.; Hubert, L. G. *J. Mater. Chem.* **2002**, *12*, 2519.

(12) (a) Cavani, F.; Trifiró, F.; Vaccari, A. *Catal. Today* **1991**, *11*, 173. (b) Rives, V. *Layered Double Hydroxides: Present and Future*; Nova Sci. Pub.: New York, 2001. (c) Wypych, F.; Satyanarayana, K. G. *Clay Surface: Fundamentals and applications*; Elsevier (Academic): London, 2004. (d) Auerbach, S. M.; Carrado, K. A.; Dutta P. K. *Handbook of layered materials*; M. Dekker Inc.: New York, 2004. (e) Evans, D. G.; Slade, R. C. T. *Struct. Bonding (Berlin)* **2006**, *119*, 1. (f) Li, F.; Duan, X. *Struct. Bonding (Berlin)* **2006**, *119*, 193.

(13) Vucelic, M.; Jones, W.; Moggridge, G. D. *Clays Clay Miner.* **1997**, *45*, 803.

(14) Zou, L.; Li, F.; Xiang, X.; Evans, D. G.; Duan, X. *Chem. Mater.* **2006**, *18*, 5852.

Transmission electron microscopy (TEM) images were recorded with a Philips TECNAI-20 high-resolution transmission electron microscope. The accelerating voltage was 200 kV.

The specific surface area of the sample was measured using the Brunauer−Emmett−Teller (BET) method using a Quantachrome Autosorb-1C-VP analyzer. Prior to the measurements, samples were degassed at 200 °C for 2 h.

X-ray photoelectron spectra (XPS) was recorded on a Thermo VG ESCALAB250 X-ray photoelectron spectrometer at a pressure of about 2×10^{-9} Pa using Al Kα X-rays as the excitation source. The binding energy (BE) calibration of the spectra has been referred to the carbon 1s peak, located at BE = 284.8 eV.

Solid-state UV–vis diffuse reflectance spectra were recorded at room temperature and in the air by means of a Shimadzu UV-2501PC spectrometer equipped with an integrating sphere attachment using $BaSO_4$ as background.

The photoluminescence (PL) measurement was carried out by using a Shimadzu RF PC-5301 spectrofluorophotometer at room temperature. A 150 W xenon lamp was used as the excitation source.

The EPR experiment was performed at room temperature by using a Bruker E-500 spectrometer operated in the X band (9.77 GHz) with 100 kHz field modulation. The power and amplitude modulation are 12.7 mW and 0.1 mT, respectively.

^{71}Ga solid-state magic-angle spinning (MAS) NMR spectra were recorded at 121.98 MHz with a pulse width of 0.4 μs on a Varian Infinity Plus 400 spectrometer under an external magnetic field of 9.4 T. The samples, held in 4.0 mm zirconia rotors, were spun at 9.0 or 9.5 kHz. The acquisition delay between successive pulses to avoid saturation effects was 10 μs. All measurements were made at room temperature, and $Ga(H_2O)_6^{3+}$ was used as the external standard.

The Ga K-edge EXAFS measurements of $ZnGa_2O_4$ powers were performed at the beamline of U7C of the National Synchrotron Radiation Laboratory (Hefei, China). The electron beam energy of the Photon Factory was 0.8 GeV, and the maximum stored current was 300 mA. The hard X-ray beam was from a three-pole superconducting wiggler with a magnetic field intensity of 6 T. Fixed-exit Si(111) flat double crystals were used as the monochromator. The energy resolution was about 2–3 eV by using the Cu foil 3d near K-edge feature. The X-ray harmonics were minimized by detuning the two flat Si(111) crystal monochromators to about 70% of the maximum incident light intensity. Ionization chambers filled with Ar/N_2 mixed gases were used to collect the EXAFS spectra in transmission mode at room temperature.

Results and Discussion

Synthesis and Characterization of the ZnGa−LDH precursor. Figure 1 illustrates the powder XRD pattern of the carbonate-containing ZnGa−LDH precursor. It can be noted that the XRD pattern exhibits the characteristic diffraction of hydrotalcite (HT)-like materials[15] with a series of (00*l*) peaks at a low angle corresponding to the basal spacing and higher-order diffractions; no other crystalline phases are present. The strong and sharp diffractions reveal that the LDH precursor consists of a well-crystallized single phase with large constituting crystallites. Analysis of the as-synthesized precursor by ICP-ES as well as TG gives the following chemical composition: $[Zn_{0.77}Ga_{0.23}(OH)_2]$

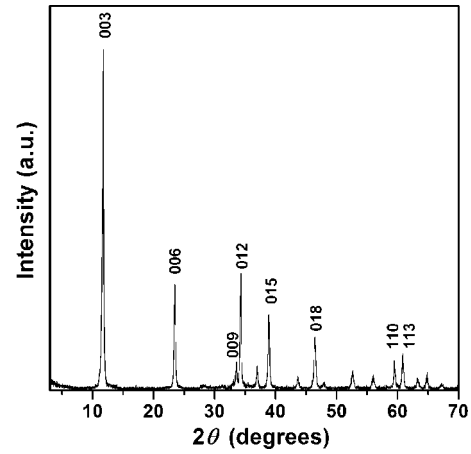

Figure 1. Powder XRD pattern of the ZnGa-LDH precursor.

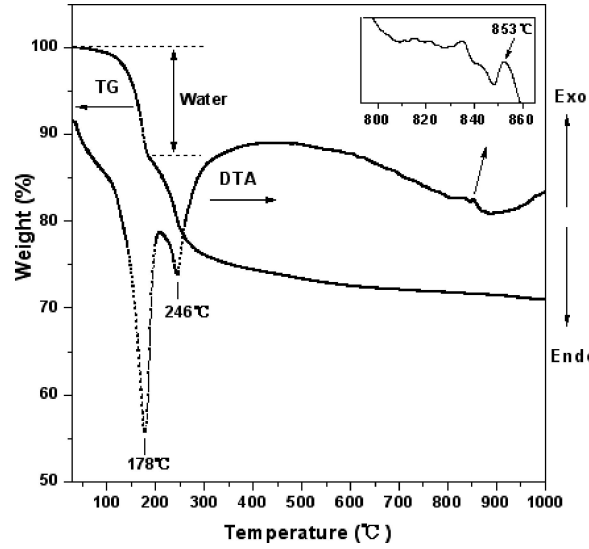

Figure 2. TG-DTA curves of the ZnGa-LDH precursor. (The exothermic peak at around 853 °C seems slight due to the existence of an extremely strong endothermic peak at 178 °C.)

$(CO_3)_{0.115}{\cdot}0.82H_2O$, indicating that the Zn/Ga molar ratio in the precursor is similar to that in the initial synthesis mixture.

The thermal behavior of the as-synthesized ZnGa−LDH precursor was examined by simultaneous TG/DTA analysis (Figure 2). As usual, the weight loss occurs essentially in two steps:[16] the first one (12 wt %) at low temperatures (*ca.* 40–185 °C) corresponds to the removal of water physisorbed on the external surface of the crystallites as well as water intercalated in the interlayer galleries; the second weight loss (14 wt %) at higher temperatures (*ca.* 185–395 °C) involves dehydroxylation of the layers as well as removal of the volatile species (CO_2) arising from the interlayer carbonate anions. Two obvious endothermic peaks recorded at around 178 and 246 °C in the DTA curves correspond to the two weight loss steps. Moreover, the slight exothermic peak at around 853 °C, without any weight loss accompanied, should be attributed to the rapid formation of $ZnGa_2O_4$ spinel.

Synthesis of $ZnGa_2O_4$ Spinel. Figure 3 shows the powder XRD patterns of the calcined ZnGa−LDH precursor at 900

(15) Busetto, C.; Del Piero, G.; Mamara, G.; Trifiró, F.; Vaccari, A. *J. Catal.* **1984**, *85*, 260.

(16) Zhao, Y.; Li, F.; Zhang, R.; Evans, D. G.; Duan, X. *Chem. Mater.* **2002**, *14*, 4286.

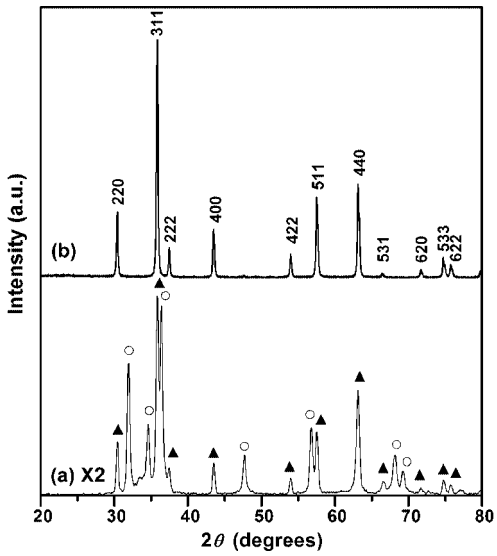

Figure 3. Powder XRD patterns of (a) calcined ZnGa-LDH at 900 °C for 6 h and (b) the corresponding $ZnGa_2O_4$ spinel obtained by the removal of ZnO from the calcined LDHs by selective leaching. (○) ZnO zincite; (▲) $ZnGa_2O_4$ spinel.

°C for 6 h and the corresponding $ZnGa_2O_4$ spinel obtained after selective leaching of ZnO from the calcined precursor with an aqueous alkali solution. It can be obviously noticed that calcination at 900 °C has destroyed the layered structure of the precursor, and that the characteristic X-ray diffraction peaks of ZnO (zincite) and $ZnGa_2O_4$ spinel phases appear. The powder XRD pattern of the treated solids with aqueous alkali solution (Figure 3b) reveals that the ZnO phase has been completely removed and that only the spinel phase remains. Elemental analysis by ICP-ES gives a Zn/Ga atomic ratio of 0.50–0.52 in the $ZnGa_2O_4$ spinel samples, indicating that removal of the ZnO phase in the calcined precursor is essentially complete. All diffraction peaks can be exactly indexed to the cubic spinel $ZnGa_2O_4$ phase (JCPDS No. 38-1240) with a lattice parameter of $a = 0.8323$ nm, which is slightly higher than the calculated value of $a = 0.8310$ nm for $ZnGa_2O_4$ spinel by the solid-state method (Supporting Information, Figure S1). This slight discrepancy is indicative of the structural difference in $ZnGa_2O_4$ spinels prepared by two routes. The presence of the spinel structure is also confirmed by FT-IR spectroscopy (Supporting Information, Figure S2), where there are two strong characteristic absorption peaks of Zn−O and Ga−O metal–oxygen vibrations at about 575 and 417 cm^{-1}, respectively.[7c] In addition, EDX analysis on $ZnGa_2O_4$ spinel by the precursor route (Supporting Information, Figure S3) shows that the sample contains no detectable contaminative element except desired Zn, Ga, and O, and the atomic ratio of Ga/Zn is very close to 2:1, in agreement with the above ICP elemental analysis results.

The above observations indicate that $ZnGa_2O_4$ spinel can be successfully prepared by the ZnAl−LDH precursor route at a lower calcination temperature and shorter calcination time compared with the conventional solid-state reaction method (at 1000 °C for 16 h or 1300 °C for 5 h).[1,3,5b,6,8] This is due to the several advantages that LDHs possess as a precursor to spinels.[14,17] A uniform distribution of metal cations on the atomic level without a segregation of "lakes" of separate cations within the brucite-like layers, which ensures the high homogeneity in a *single-source* ZnGa−LDH precursor, facilitates the crystallization of a spinel phase upon calcination. The close structural relationship between the LDH precursor and its calcination product is also a key factor. The formation of a spinel from an LDH precursor has been described as a topotactic process, in which the (110) reflection of the LDH transforms to the (440) reflection of the spinel.[17a] Further, since solid–solid diffusion is the rate-limiting step in traditional solid-state reactions, this alternative approach is successful because it completely eliminates atomic diffusion distances and allows the precursor to be thermally transformed rapidly into a predesigned $ZnGa_2O_4$ product phase at relatively low temperatures, leading to a lower chance of side reactions, such as ZnO volatilization, which would give nonstoichiometric products.

The morphology of the obtained $ZnGa_2O_4$ spinel was determined by SEM and TEM experiments. As shown in Figure 4a, the $ZnGa_2O_4$ product exhibited a compact arrangement of uniform nanocrystallites. According to the higher-magnification SEM image (Figure 4b) and TEM image (Figure 4c) of the $ZnGa_2O_4$ spinel, the average particle size is estimated to be around 150 nm, much smaller than that of the $ZnGa_2O_4$ spinel prepared by the solid-state method (Supporting Information, Figure S4). Considering that particle growth is controlled by the boundaries between particles,[18] one can assume that the mean boundry velocity, ν, is proportional to the thermodynamic driving force, ΔF, applied to it:

$$\nu = M\Delta F \quad (1)$$

where M is the particle-boundary mobility, which depends on the meachnism of diffusion (a kinetic parameter in eq 1). Therefore, two different approaches including a decrease of particle boundary mobility and a reduction of ΔF can be used to prevent particle growth. In our system, the large amounts of ZnO particles around, which are 5 times that of $ZnGa_2O_4$ spinel in the calcined mixture, will obviously reduce the $ZnGa_2O_4$ particle-boundary mobility during the calcination process. And for the thermodynamic driving force ΔF, the decrease may also exist when large amounts of ZnO particles are around the target $ZnGa_2O_4$ spinel particles. Such a decrease in ΔF has already been confirmed by experimental and theoretical evidence in metal solid solution systems.[19] As a result, one can deduce that the ZnO particles generated during the calcination have a remarkable segregation and inhibition effect on the growth of $ZnGa_2O_4$ spinel. This means that the $ZnGa_2O_4$ spinel nanocrystallites were confined in the voids formed by the self-generated highly dispersed ZnO as a sacrificial template and were prevented from

(17) (a) Bellotto, M.; Rebours, B.; Clause, O.; Lynch, J.; Bazin, D.; Elkaim, E. *J. Phys. Chem.* **1996**, *100*, 8535. (b) Liu, J.; Li, F.; Evans, D. G.; Duan, X. *Chem. Commun.* **2003**, 542. (c) Li, F.; Liu, J.; Evans, D. G.; Duan, X. *Chem. Mater.* **2004**, *16*, 1597.

(18) Chiang, Y. M.; Birnie, D. P., III; Kingery, W. D. *Physical Ceramic-Principles for Ceramic Science and Engineering*; John Wiely and Sons: New York, 1997.

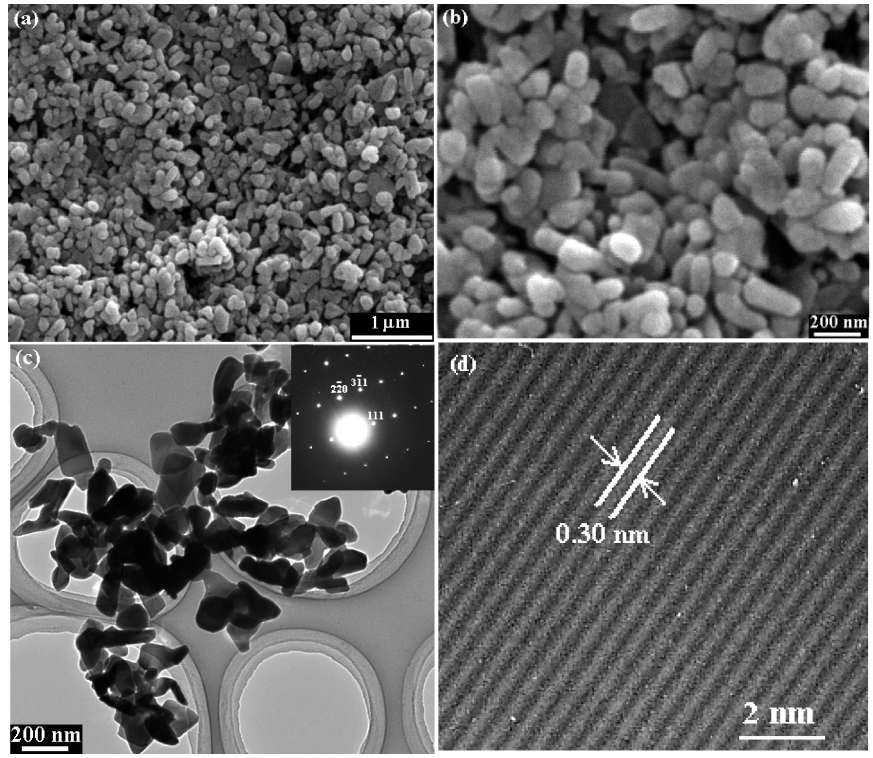

Figure 4. (a) Typical SEM image of $ZnGa_2O_4$ spinel by precursor route; (b) magnified image of $ZnGa_2O_4$ spinel by precursor route; (c) typical TEM image of $ZnGa_2O_4$ spinel by precursor route and the electron diffraction pattern (inset); (d) HRTEM image of $ZnGa_2O_4$ spinel by precursor route.

recrystallizing/sintering at elevated temperatures. The result is also in good agreement with the fact that the surface area of as-prepared $ZnGa_2O_4$ spinel measured by a BET method using nitrogen at 77 K was 12.1 $m^2\ g^{-1}$, much larger than that of $ZnGa_2O_4$ prepared by the solid-state method (1.7 $m^2\ g^{-1}$).

Additionally, in order to investigate the influence of the Zn^{2+}/Ga^{3+} molar ratio in a precursor upon the formation of $ZnGa_2O_4$ spinel, $ZnGa_2O_4$ was also prepared by calcining the ZnGa−LDH with an initial Zn^{2+}/Ga^{3+} molar ratio of 2.0. Accordingly, the estimated amount of ZnO is 3 times that of $ZnGa_2O_4$ spinel in the calcined mixture. It can be noted from the SEM image of obtained $ZnGa_2O_4$ (Supporting Information, Figure S5) that the sample exhibited a compact arrangement of nanocrystallites but with a larger particle size and less uniform particle size distribution than that obtained from ZnGa−LDH with a Zn^{2+}/Ga^{3+} molar ratio of 3.0. This is because a smaller amount of ZnO shows a less remarkable segregation and inhibition effect on the growth of $ZnGa_2O_4$ spinel.

The HRTEM and SAED analysis also provides more detailed structural information about the $ZnGa_2O_4$ spinel. The SAED pattern taken from several individual particles (a typical pattern in the inset of Figure 4c) reveals that $ZnGa_2O_4$ consists of a single-crystal cubic spinel structure. Moreover, a typical atomic-resolved image of an individual $ZnGa_2O_4$ crystallite (Figure 4d) indicates that the measured spacing of the crystallographic planes is 0.30 nm, which agrees well with the separation between the (220) lattice planes and further supports the single-crystalline nature of the particles. $ZnGa_2O_4$ spinels with small particle sizes have also been prepared by sol–gel and hydrothermal methods. For example, the sol–gel powders begin to crystallize at 500 °C, and a pure $ZnGa_2O_4$ spinel phase is obtained at 700 °C. However, a Ga_2O_3 phase may appear at higher calcination temperatures (above 800 °C).[7c,11b] The hydrothermal synthesis at temperatures above 180 °C has been applied to prepare $ZnGa_2O_4$ crystals with many shapes, but in some cases, a small amount of ZnO, GaO(OH), and so on can be detected, or the particle size is not quite uniform.[10]

Structural Properties of $ZnGa_2O_4$ Spinel. The surface/near-surface chemical states of the obtained $ZnGa_2O_4$ sample by the precursor route are analyzed using XPS within a range of binding energies of 0–1200 eV (Figure 5a). Core levels of Zn 2p, Ga 2p, and O 1s can be identified, and no contaminant species are detectable within the sensitivity of the technique. Only a very low peak from absorbed carbon is present on the spectra. The fine spectra of the Ga 2p, Zn 2p, and O 1s peaks are displayed in Figure 5b, c, and d, respectively. In addition, the energetic separation between the Zn $2p_{2/3}$ and Ga $2p_{2/3}$ peaks (ΔE) can be used as a sensitive tool to distinguish between a complete formation of $ZnGa_2O_4$ spinel corresponding to a low ΔE value and a physical mixture of metal oxide powers.[8b] Here, the ΔE value for $ZnGa_2O_4$ spinel obtained by the precursor route at 900 °C for 6 h (96.0 eV) is lower than that for $ZnGa_2O_4$ spinel obtained by the solid-state reaction at 1100 °C for 24 h (96.3 eV),[8b] reflecting more complete conversion to the spinel for the LDH precursor as a consequence of the uniform distribution of Zn^{2+} and Ga^{3+} cations within the precursor as well as the native interaction between metal ions.

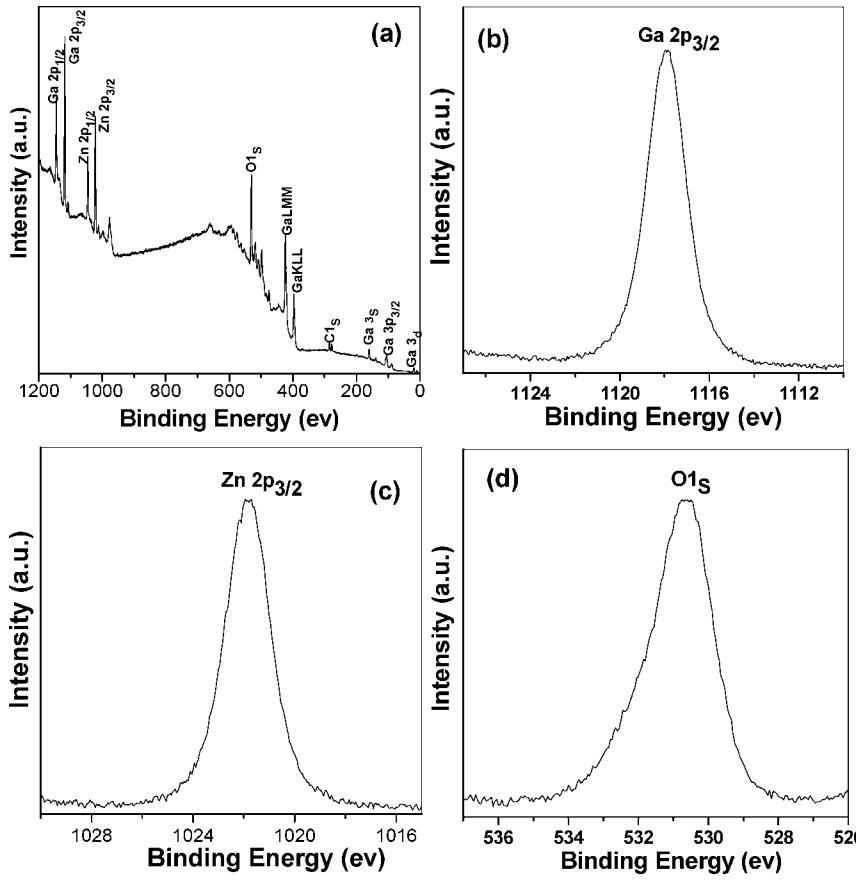

Figure 5. XPS spectra of $ZnGa_2O_4$ spinel by precursor route: (a) survey, (b) Ga 2p, (c) Zn 2p, and (d) O 1s.

Solid-state NMR is a good tool for analyzing the coordination environment of many ions in solid-state materials. ^{71}Ga is a quadrupolar nucleus ($I = 3/2$), and its NMR spectra are generally affected by strong quadrupolar broadening arising from the interaction of the nuclear quadrupolar momentum with the electric field tensor at the nucleus position. However, there are also reports about the successful identification of tetrahedrally coordinated gallium (Ga_T) and octahedrally coordinated gallium (Ga_O) at different chemical shifts.[20] The spinel structure, AB_2O_4, can be described in terms of a close-packed cubic arrangement of anions with one-half the octahedral holes and one-eighth of the tetrahedral holes filled with cations. It is generally considered that $ZnGa_2O_4$ is a normal spinel, where Zn^{2+} and Ga^{3+} ions occupy the tetrahedrally and octahedrally coordinated sites, respectively, due to the fact that Zn^{2+} ions usually have no octahedral stabilization energy.[21] Accordingly, the inversion parameter in $ZnGa_2O_4$ spinel, $\gamma = Ga_{Td}:(Ga_{Td} + Ga_{Oh})$, is 0. The ^{71}Ga MAS NMR spectra of the $ZnGa_2O_4$ spinel products by two routes are shown in Figure 6. To the best of our knowledge, no one has previously employed ^{71}Ga MAS NMR to identify the Ga^{3+} coordination environment in $ZnGa_2O_4$ spinel. From the spectra, the presence of both tetrahedral GaO_4 sites (chemical shift at $\sim$73 ppm) and octahedral GaO_6 sites (chemical shift at ~ -33 ppm) is unequivocally determined. This result seems to be inconsistent with the previous viewpoint that $ZnGa_2O_4$ is a normal spinel with an inversion parameter of 0. This is because the inversion parameter of spinel materials also depends on its synthesis conditions. For example, there are a few reports about the existence of tetrahedrally coordinated Al^{3+} ions in zinc aluminate ($ZnAl_2O_4$) spinels with an inversion degree up to 0.15,[14,22] though $ZnAl_2O_4$ is generally considered as a nomal spinel.

In addition, on the basis of a detailed comparison of the ^{71}Ga MAS NMR spectra, it could be found that the occupancy extent of tetrahedral sites by Ga^{3+} cations shows a marked difference between two $ZnGa_2O_4$ spinel products by different routes. The inversion parameter, calculated from the tetrahedral to octahedral peak area ratio, is about 0.30 for $ZnGa_2O_4$ spinel by the precursor route and 0.17 for $ZnGa_2O_4$ spinel by the solid-state method. Therefore, it is concluded that $ZnGa_2O_4$ products by the precursor route and the solid-state method are not perfectly normal spinel,

(19) Gleiter, H. *Acta Mater.* **2000**, *48*, 1.
(20) (a) Aramendía, M. A.; Borau, V.; Jiménez, C.; Marinas, J. M.; Romero, F. J.; Ruiz, J. R. *J. Solid State Chem.* **1997**, *131*, 78. (b) Aramendía, M. A.; Avilés, Y.; Borau, V.; Luque, J. M.; Marinas, J. M.; Ruiz, J. R.; Urbano, F. J. *J. Mater. Chem.* **1999**, *9*, 1603. (c) Aramendía, M. A.; Avilés, Y.; Benítez, J. A.; Borau, V.; Jiménez, C.; Marinas, J. M.; Ruiz, J. R.; Urbano, F. J. *Microporous Mesoporous Mater.* **1999**, *29*, 319. (d) Lavalley, J. C.; Daturi, M.; Montouillout, V.; Clet, G.; Areán, C. O.; Delgado, M. R.; Sahibed-dine, A. *Phys. Chem. Chem. Phys.* **2003**, *5*, 1301.
(21) Well, A. F. *Structural Inorganic Chemistry*, 5th ed.; Oxford University Press: Oxford, 1984; p 595.
(22) (a) Kapoor, P. N.; Heroux, D.; Mulukutla, R. S.; Zaikovskii, V.; Klabunde, K. J. *J. Mater. Chem.* **2003**, *13*, 410. (b) Mathur, S.; Veith, M.; Haas, M.; Shen, A.; Lecerf, N.; Huch, V.; Hufner, S.; Haberkorn, R.; Beck, H. P.; Jilavi, M. *J. Am. Ceram. Soc.* **2001**, *84*, 1921.

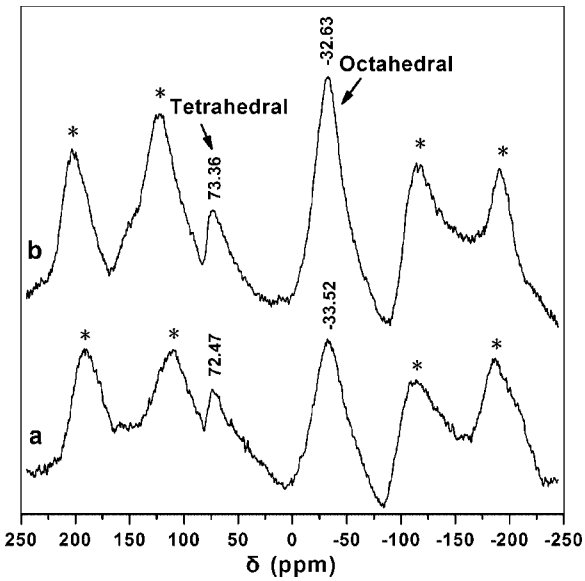

Figure 6. ^{71}Ga MAS NMR spectra for $ZnGa_2O_4$ spinel obtained by (a) the precursor route and (b) the solid-state reaction method. Asterisks denote spinning sidebands.

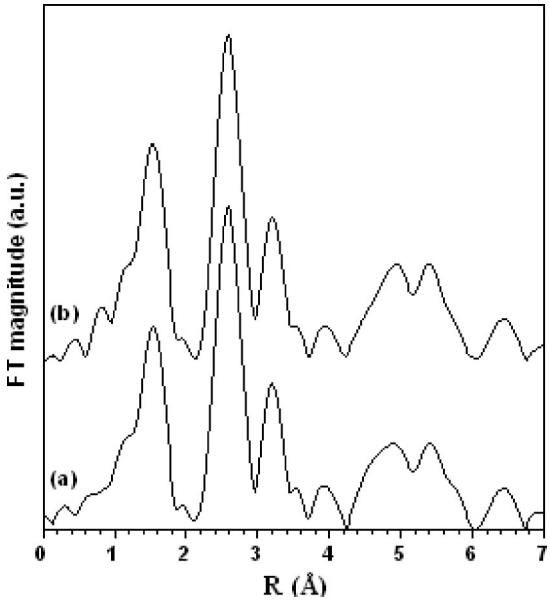

Figure 7. Moduli of the Fourier transform at Ga K edge for $ZnGa_2O_4$ spinel obtained by (a) the precursor route and (b) the solid-state reaction method.

and they could be written as $(Zn_{0.70}Ga_{0.30})[Zn_{0.30}Ga_{1.30}]O_4$ and $(Zn_{0.83}Ga_{0.17})[Zn_{0.17}Ga_{1.83}]O_4$, respectively, where the round and square brackets denote cation sites with tetrahedral and octahedral coordination.

The X-ray absorption fine structure technique is a powerful tool for determining the local structure of materials due to its sensitivity to the short-range order and atomic species surrounding the absorbed atom. Figure 7 shows the moduli of the Fourier transform at the Ga K-edge of $ZnGa_2O_4$ spinels. Peaks appearing at 1–2 Å are due to backscattering from the adjacent oxygen atoms, and peaks at 2–3 Å show the presence of the second-neighboring metal atoms (Ga or Zn atoms). Figure 8 displays the experimental (solid) and fitted (dotted) EXAFS curves with the k^3 weight for Ga−O

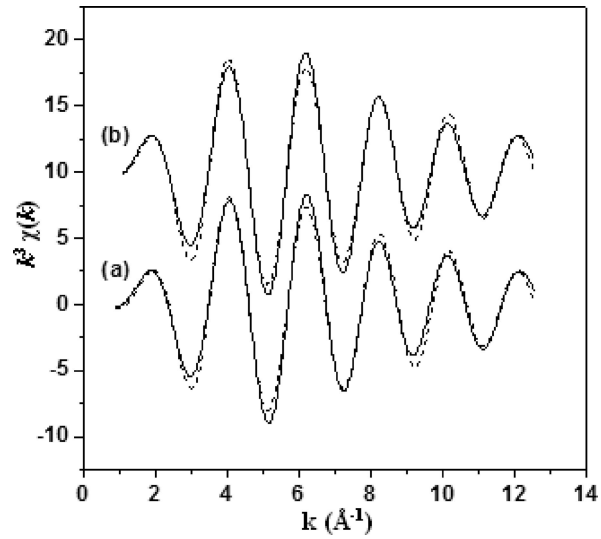

Figure 8. Experimental (solid line) and fitting (dot line) EXAFS curves with k^3 weight of Ga−O coordination for $ZnGa_2O_4$ spinel obtained by (a) the precursor route and (b) the solid-state reaction method.

Table 1. Local Coordination Parameters Around Ga in $ZnGa_2O_4$ Spinel by Different Methods

method	$N_{Ga-O}{}^a$	$R_{Ga-O}{}^b$/Å	$\sigma^2_{Ga-O}{}^c$/Å^2
solid-state method	5.9(5)	1.94(3)	0.0047
precursor route	5.6(6)	1.94(0)	0.0049

^{a} N = coordination number. ^{b} R = interatomic distance. ^{c} σ = Debye–Waller factor.

coordination in the $ZnGa_2O_4$ spinel. The fitting parameters are listed in Table 1. Data analysis suggests the shortening Ga−O distance and the reducing Ga−O coordination number in $ZnGa_2O_4$ spinel obtained by the precursor route, which further confirmed the existence of tetrahedral Ga^{3+} centers in the $ZnGa_2O_4$ spinel lattice, and is in agreement with the solid-state NMR results to some extent.

Optical Properties of $ZnGa_2O_4$ Spinel. UV–vis absorption measurement is a convenient and effective method for explaining some important features concerning the band structures of semiconductor materials. By analysis of absorption coefficients for $ZnGa_2O_4$ phosphors, the so-called optical energy gaps can be estimated using a classical Tauc approach.[23] Figure 9 shows the Tauc plot $(\alpha E_p)^2$ versus E_p for $ZnGa_2O_4$ phosphors obtained by the precursor route and solid-state method. It has been well-established that, for a large number of semiconductors, the dependence of the absorption coefficient α, for the high-frequency region, upon the photon energy E_p, for optically induced transitions, is given by the following expression:[23]

$$\alpha E_p = K(E_p - E_g)^n \quad (2)$$

where E_g represents the optical band gap, E_p is the photon energy, K is a constant, and n depends on the nature of the transition. In fact, n assumes a value of $^1/_2$, $^3/_2$, 2, and 3 for allowed direct, forbidden direct, allowed indirect, and forbidden indirect transitions, respectively. In the present case, the best fit of $(\alpha E_p)^2$ versus E_p was obtained for $n = {}^1/_2$, suggesting the allowed direct transitions across the energy

(23) Patil, P. S.; Kadam, L. D.; Lokhande, C. D. *Thin Solid Films* **1996**, *272*, 29.

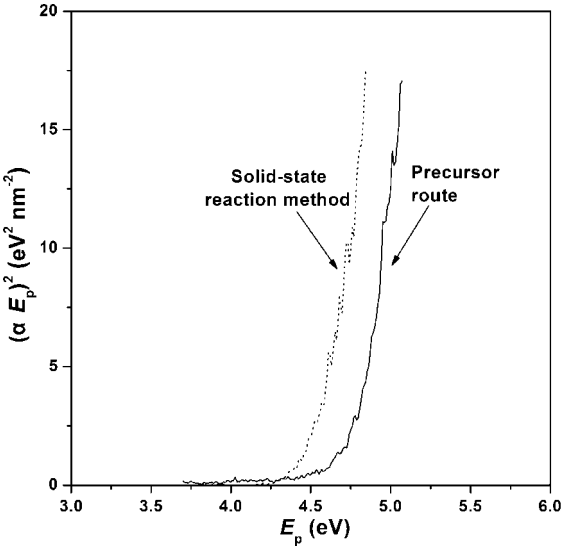

Figure 9. Tauc plot for $ZnGa_2O_4$ spinel obtained by the precursor route (solid line) and the solid-state reaction method (dotted line).

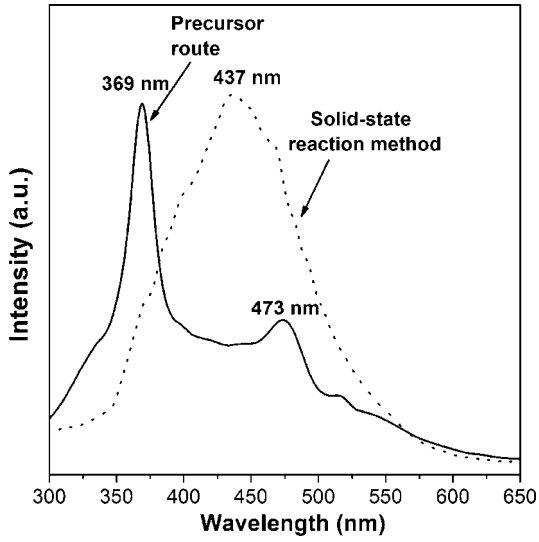

Figure 10. Room-temperature photoluminescence PL spectra of $ZnGa_2O_4$ spinel obtained by the precursor route (solid line) and the solid-state reaction method (dotted line) excited at a wavelength of 240 nm.

band gap of $ZnGa_2O_4$ phosphors. The extrapolated value (the straight lines to the x axis) of E_p at $\alpha = 0$ gives absorption edge energies corresponding to $E_g = 4.77$ and 4.47 eV, respectively, for $ZnGa_2O_4$ phosphors obtained by the precursor route and solid-state method. These two values, particularly for $ZnGa_2O_4$ phosphor by the solid-state method, are close to the value for bulk $ZnGa_2O_4$ (4.4 eV). It is generally accepted that the band gap energy is proportional to the bond length.[6b] Therefore, the above moving of the optical band gap ($\Delta E_g = 0.3$ eV) should result from the shortening bond length of Ga−O in the $ZnGa_2O_4$ spinel obtained by the precursor route.

Figure 10 shows the room-temperature PL spectra of $ZnGa_2O_4$ phosphors. Like most previous reports, $ZnGa_2O_4$ phosphor by the solid-state method exhibits a broad emission band in the range of 350−600 nm with a maximum emission peak at 437 nm. However, $ZnGa_2O_4$ phosphor from the precursor route shows two emission bands: a strong UV emission centered at 369 nm and a weak emission centered at 473 nm. Generally, bulk $ZnGa_2O_4$ phosphors exhibit the characteristic blue emission around 430 nm from the self-activation center of Ga−O groups,[6] which explains well the luminescence properties of $ZnGa_2O_4$ phosphor by the solid-state method. The weak emission at 473 nm possibly results from the deep-level defect.

Generally, the luminescence of the $ZnGa_2O_4$ phosphor is ascribed to Ga−O transition, and thus two different viewpoints explain the origin of UV emission centered at around 360 nm. One is due to the existence of oxygen vacancies, resulting in the change of the self-activated luminescent center's environment for blue emission arising from octahedral Ga−O groups in the spinel lattice.[24] Another one proposed by Jeong et al. is from the new self-activated centers of tetrahedral Ga−O groups in the spinel lattice.[6b] However, the latter has not been confirmed directly by experiments. In our study system, the room-temperature EPR spectrum of $ZnGa_2O_4$ phosphor by the precursor route (Supporting Information, Figure S6) indicates that no EPR signal around 3550 G responsible for oxygen vacancies exists. The absence of oxygen vacancies in $ZnGa_2O_4$ is because as-prepared $ZnGa_2O_4$ is prepared by heat treatment in an air atmosphere, and the high crystal quality of $ZnGa_2O_4$ can decrease the impurities and structure defects including oxygen vacancies.[25] Furthermore, it is noted that ^{71}Ga MAS NMR experiments confirm the existence of a high proportion of tetrahedral Ga sites in the $ZnGa_2O_4$ sample by the precursor route. Although tetrahedral Ga−O groups also exist in the structure of $ZnGa_2O_4$ phosphor when using the solid-state method, UV luminescence at 360 nm does not take place. This is because of the fact that, in view of crystal field, the tetrahedral symmetry is less than the octahedral symmetry. Accordingly, the higher proportion of tetrahedrally coordinated Ga^{3+} ions in $ZnGa_2O_4$ spinel by the precursor route may lead to a significant decrease of crystal field, and thus the blue shift in the emission spectra with strong UV-emitting properties.

Conclusions

In summary, we report the preparation of single-crystalline $ZnGa_2O_4$ spinel with intense ultraviolet emission using a single-source inorganic precursor approach without the use of organic reagents. The obtained $ZnGa_2O_4$ phosphor consists of small homogeneous particles, while its formation requires a lower temperature and shorter calcination time, compared with that of the solid-state method. The ZnO generated during the calcination of the precursor acts as a sacrificial template and exhibits an excellent segregation and inhibition effect on the growth of $ZnGa_2O_4$ spinel. Detailed structural analysis shows that the increased band gap energy (0.3 eV) results from the shortening of the Ga−O bond length in the $ZnGa_2O_4$

(24) (a) Kim, J. S.; Kang, H. I.; Kim, W. N.; Kim, J. I.; Choi, J. C.; Park, H. L.; Kim, G. C.; Kim, T. W.; Hwang, Y. H.; Mho, S. I.; Jung M.-C.; Han, M. *Appl. Phys. Lett.* **2003**, *82*, 2029. (b) Kim, J. S.; Kang, H. I.; Chon, C. M.; Moon, H. S.; Kim, T. W. *Solid State Commun.* **2004**, *129*, 163.
(25) Cao, H.; Qiu, X.; Liang, Y.; Zhu, Q.; Zhao, M. *Appl. Phys. Lett.* **2003**, *83*, 761.

spinel obtained by the precursor route. Moreover, it is found that two kinds of Ga−O groups (tetrahedral and octahedral) simultaneously exist in the $ZnGa_2O_4$ spinel structure, and the Ga−O coordination environment has a great influence on the photoluminence of $ZnGa_2O_4$ phosphors.

Acknowledgment. The authors gratefully acknowledge financial support from the National Science Foundation of China (20631040), Program for Changjiang Scholars and Innovative Research Team in University (PCSIRT 0406), the 111 Project (B07004), and the Program for New Century Excellent Talents in University (NCET-04-0120). They also acknowledge the National Synchrotron Radiation Laboratory (NSRL) for provision of synchrotron radiation facilities and thank Dr. Shiqiang Wie, Bo He, and Zhi Xie for assistance in using beamline U7C.

Supporting Information Available: Figures illustrating the results of analyses done in the study. This material is available free of charge via the Internet at http://pubs.acs.org.

IC7012528